Graphical abstract

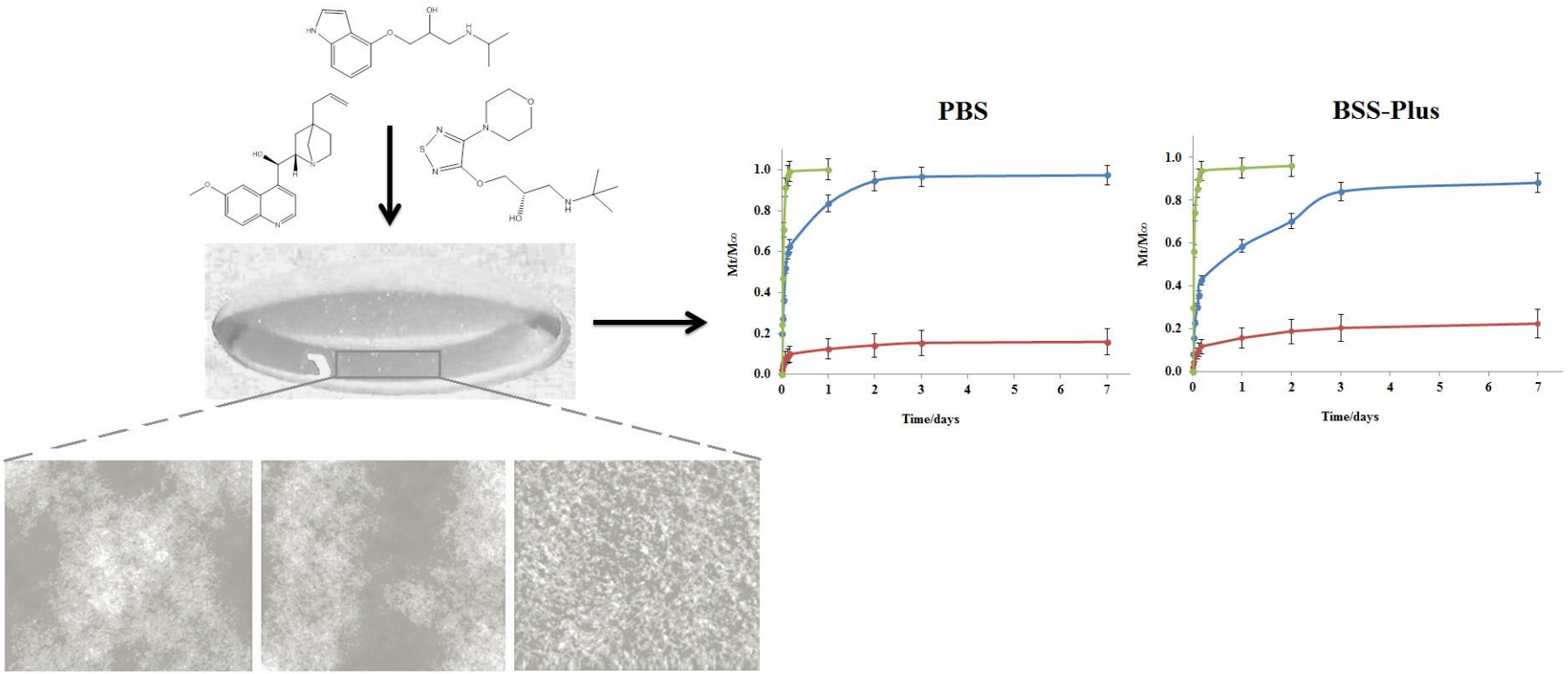

Sustained and controlled release of lipophilic drugs from a self-assembling amphiphilic peptide hydrogel

Maria-Lucia Briuglia[1], Andrew J. Urquhart[2], Dimitrios A. Lamprou[1*]

[1] *Strathclyde Institute of Pharmacy and Biomedical Sciences (SIPBS), University of Strathclyde, 161 Cathedral Street, Glasgow, G4 0RE, Scotland, UK.*
[2] *Department of Micro- and Nanotechnology, Technical University of Denmark, Ørsteds Plads 2800 Kgs. Lyngby, Denmark.*

*Corresponding author: Tel: +44(0)141 548 4968, E-mail: dimitrios.lamprou@strath.ac.uk

Keywords: controlled release, amphiphilic hydrogels, spectroscopy, AFM, lipophilic drugs.

Abstract

Materials which undergo self-assembly to form supermolecular structures can provide alternative strategies to drug loading problems in controlled release application. RADA 16 is a simple and versatile self-assembling peptide with a designed structure formed of two distinct surfaces, one hydrophilic and one hydrophobic that are positioned such a well-ordered fashion allowing precise assembly into a predetermined organization. A "smart" architecture in nanostructures can represent a good opportunity to use RADA16 as a carrier system for hydrophobic drugs solving problems of drugs delivery. In this work, we have investigated the diffusion properties of Pindolol, Quinine and Timolol Maleate from RADA16 in PBS and in BSS-PLUS at 37 °C. A sustained, controlled, reproducible and efficient drug release has been detected for all the systems, which has allow to understand the dependence of release kinetics on the physicochemical characteristics of RADA16 structural and chemical properties of the selected drugs and the nature of solvents used. For the analysis various physicochemical characterization techniques were used in order to investigate the state of the peptide before and after the drugs were added. Not only does RADA16 optimise drug performance, but it can also provide a solution for drug delivery issues associated with lipophilic drugs.

1. Introduction

Hydrogels are cross-linked hydrophilic polymer networks that can absorb more than 100 times their dry weight in water, giving them physical characteristics similar to soft tissue [Gibas et al., 2010]. Self-assembling peptide hydrogels are an important class of hydrogels, which are potentially excellent materials for various molecular controlled release applications [Nagai et al., 2006]. Self-assembly is a spontaneous process by which several individual molecules are associated into a coherent and organized structure under thermodynamic equilibrium conditions by non-covalent interaction, such as ionic and hydrogen bonding [Zhang et al., 1993; Jun et al., 2004; Zhaoyang et al. 2008]. In comparison with chemically synthesized polymer materials, self-assembling peptide hydrogels have numerous advantages, for example, (i) the peptides that construct the hydrogels can often be degraded in vivo, and the resulting products (amino acids) are nontoxic; (ii) the hydrogels are spontaneously formed without using harmful chemicals such as cross-linkers; (iii) the spontaneous process allows for an solution-gel transformation in vivo by injecting peptide solutions at specific locations, and it also enables a facile incorporation of cell-specific bioactive moieties into hydrogels; (iv) the peptide building blocks represent a variety of chemical groups that allow hydrogels to be easily modified with chemical and biological moieties; and (v) the hydrogel maintains a high water content, which may allow for the diffusion of a wide range of molecules [Zhang et al.,2002; Zhang, 2003; Huang et al., 2011]. Peptide hydrogels have been demonstrated to be useful as controlled release devices [Nagai et al., 2006; Koutsopoulos et al., 2008]. Depending on molecular design, many different hydrogels (e.g. P11-family [Aggeli et al., 2003; Carrick et al., 2007], MAX8 [Altunbas et al.,2011], Fmoc-FF with KGM [Jayawarna et al., 2009], EAK16 [Keyes et al., 2004] and RADA16 [Gelain et al., 2010]) have been constructed. For our study we have used RADA16 which has a high propensity to self-assemble into hydrogels with nanofibre structures containing ~99.5% w/v water ensuring the biodegradability [Arosio et al., 2012]. RADA16, known as "molecular Lego" [Zhang, 2002], has two surfaces – one hydrophilic composed of alternating arginine (positive charge) and aspartic acid (negative charge), and one hydrophobic surface enabling formation of supra-molecular assemblies by a "lock and fit" model [Nune et al., 2013]. Moreover, RADA16 contains a regular repeat of alternating hydrophobic and hydrophilic amino acids [Yokoi et al., 2005] forming a hydrogel with a large surface to volume ratio [Zhang, 2003]. Alternation of hydrophobic and hydrophilic amino acids tends to promote β-strand secondary structure and two structural features that lead to stable nanofibre formation: (1) hypothesized hydrogen bonding between neighbouring peptide backbones, stabilizing a possible cross-β structural motif well-known to describe amyloid fibrils [Jonker et al.,2012; Eanes et al., 1968] and (2) separation between hydrophobic and hydrophilic faces that are believed to form the core and surface of nanofibres, respectively [Yokoi et al.,2005]. According to previous studies [Nagai et al., 2006; Koutsopoulous et al., 2008], RADA16 is an efficient delivery carrier but has not been used for hydrophobic drugs. Therefore, we hypothesize that this "smart" architecture in nanostructure would allow loading hydrophobic drugs and permitting a sustained and controlled release providing solution for delivery problems. Therefore, we hypothesized that this "smart" architecture may encapsulate small hydrophobic molecules between peptide chains, disrupting β-sheet formation to a more α-helix configuration but permitting a sustained and controlled release providing solutions for delivery problems. In order to investigate our hypothesis, we have explored the release profiles of Pindolol (P), Quinine (Q) and Timolol maleate (T) from RADA16 hydrogel. The drug release was investigated in PBS and BSS Plus solutions at 37 °C. The developed formulations were further characterized by atomic force microscopy (AFM), circular dichroism (CD) spectrometer and Fourier transform infrared spectroscopy (FT-IR). The molecules were chosen to have a range of partition

coefficients (LogP) and acid dissociations constants (pKa).

2. Materials and Methods

2.1. Chemicals and reagents

The ac-$(RADA)_4$-$CONH_2$ peptide in 1 % solution was obtained from BD Biosciences (Bedford, MA). Pindolol (Fig.1a; Table 1a) is a nonselective β-blocker with partial β-adrenergic receptor agonist activity. Quinine (Fig.1b; Table 1b) is a natural white crystalline alkaloid having antipyretic, antimalarial, analgesic and anti-inflammatory properties. Timolol maleate salt (Fig.1c; Table 1c) is a non-selective beta-adrenergic receptor antagonist indicated for treating glaucoma, heart attacks and hypertension. All drugs were purchased from Sigma-Aldrich. Phosphate buffered saline (PBS) is an aqueous solution containing sodium chloride, sodium phosphate, and, in some formulations, potassium chloride and potassium phosphate. PBS solution was prepared using PBS buffer tablets (pH 7.4), and purchased from Sigma Aldrich. BSS-Plus is a sterile intraocular irrigating solution with pH 7.4, which was purchased from Alcon – UK. It is a complex solution with sugar and salts and it copies the physiological conditions of eyes providing an interesting study for T, which is used in glaucoma therapy. Furthermore BSS-Plus is used in this study to investigate a possible novel interaction between peptide and selected drugs due the nature of the different solvent. BSS-Plus is formed from sodium chloride 7.44 mg, potassium chloride 0.395 mg, dibasic sodium phosphate 0.433 mg, sodium bicarbonate 2.19 mg, hydrochloric acid and/or sodium hydroxide, calcium chloride dihydrate 3.85 mg, magnesium chloride hexahydrate 5 mg, dextrose 23 mg, glutathione disulfide (oxidized glutathione), 4.6 mg in water for injection.

2.2. Drug Release Experiments

Hydrogel formation occurred by mixing 200 μL of the [Ac-$(RADA)_4$-$CONH_2$] peptide solution, with 2.5 μL of drug and with 2 μl of PBS. The mixture was transferred into microcentrifuge tubes, and gelation occurred within 20 min. Subsequently, 400 μL of release medium (PBS or BSS-Plus) was slowly added to each gel mixture. Experiments were performed in triplicates. The release experiments were performed at 37 °C, for a period of 7 days, where the supernatant drugs concentration was measured at 15 min, 30 min, 1, 2, 3, 4, 24, 48, 72 h and 7 days. To satisfy the perfect-sink conditions which allow for the determination of the diffusion parameters, the supernatant was replaced with fresh PBS or BSS Plus pre-equilibrated at 37 °C at each time point. The concentration of the drug molecules inside the hydrogel and in the supernatant was determined by UV-Vis using a Varian 50 bio UV-visible spectrophotometer at room temperature. The concentration of the drug molecules released from the hydrogel was determined using a calibration curve of the pure drug molecules in PBS and BSS-Plus solutions at the wavelength where showed the maximum absorbance (Table 1). During the course of the measurements the hydrogel volume did not change.

2.3. Diffusivity determination from released drugs concentration

For a hydrogel matrix that contains a molecularly dispersed diffusing agent, the apparent diffusion coefficient was calculated by using the 1-D unsteady-state form of Fick's second law of diffusion for a plane film of thickness:

$$\frac{\delta c}{\delta t} = D\frac{\delta^2 c}{\delta x^2} \qquad \text{(Eq.1)}$$

where D is the diffusion coefficient of the active agent in the hydrogel and c is the concentration of the drug as a function of time (t) and position (x) [Frisch, 1970; Siepmann et al.,1998].

Diffusion is concentration independent and it occurs only in the positive x direction from the hydrogel to the sink. Assuming that (1) the rate at which the substance is transported to the surface is equal to the internal diffusion rate, (2) there are not solute-carrier interactions and (3) at time zero a contact between the hydrogel surface and the perfect sink is reached, Eq.(1) can be considered as [Korsmeyer et al., 1983; Ritger and Peppas, 1987; Siepmann and Peppas, 2001]:

$$\frac{M_t}{M_\infty} = \sqrt{\frac{4\,Dt}{\pi H^2}} \qquad \text{(Eq.2)}$$

M_t and M_∞ are the total mass of the diffusing compounds released after time t and infinite time, respectively.

In order to calculate the diffusion coefficient (D_0) as the drug concentration within the hydrogel approaches zero after a long diffusion time, Eq. (2) can be recast into:

$$\ln(M_\infty - M_t) = \ln\left(\frac{8\,M_\infty}{\pi^2}\right) - \theta_2 t \qquad \text{(Eq.3)}$$

$$\theta_2 = -\frac{D_0\pi^2}{H^2} \qquad \text{(Eq.4)}$$

Furthermore, the diffusion coefficient was also calculated using the Stokes-Einstein equation [Vahdat and Sullivan, 2001], which calculates the free bulk diffusion coefficient as a function of the Boltzmann constant (k_B), temperature (T), solvent dynamic viscosity (μ) and solute radius (r_H).

$$D_{S-E} = \frac{K_B T}{6\pi\mu r_H} \qquad \text{(Eq.5)}$$

k_B is the Boltzmann Constant (1.3806503 x 10^{-23} m^2 kg s^{-2} K^{-1}), T is the absolute temperature of the medium (i.e., 310 K), μ is the solvent dynamic viscosity (taken as 1.002 cP), and r_H is the hydrodynamic radius which is different for each drug.

It should be mentioned that due to the fact there exists an interaction between the solute and the nanofibres the calculated diffusivities are considered to be apparent diffusivities and allow for a comparison of the systems under study.

2.4. Dissolution data analysis

The dissolution kinetics was analysed by SigmaPlot 10.0 software (Systat Software Inc.,Chicago,IL) considering various mathematical models (Table 2) and determining the

amounts of drug released.

2.5. Atomic force microscopy (AFM)

After sonication of the ac-$(RADA)_4$-$CONH_2$ solution for 30 min, aliquots of 10 µl were removed from the peptide solution and diluted with 190 µl of water (Millipore, 18.2 MΩ cm), and left for 45 min in order to form fibres. One microliter sample was immediately deposited onto a freshly cleaved mica surface (1.5 cm x 1.5 cm; G250-2 Mica sheets 1" x 1" x 0.006"; Agar Scientific Ltd, Essex, UK) and left on the mica for 15 s, then rinsed with 100 µl of water (Millipore, 18.2 MΩ cm), air-dried, and images were acquired immediately. The images were obtained by scanning the mica surface in air under-ambient conditions using a Multimode 8 scanning probe microscope (Digital Instruments, Santa Barbara, CA, USA), operating using the new mode PeakForce QNM. The AFM measurements were obtained using ScanAsyst-air probes, for which the spring constant (0.58 N/m; nominal 0.4 N/m) and deflection sensitivity had been calibrated, but not the tip radius (the nominal value used was 2 nm). AFM images were collected from two different freshly prepared samples and at random spot surface sampling (at least seven areas per sample).

2.6. Circular dichroism (CD)

The far-UV CD spectra of the ac-$(RADA)_4$-$CONH_2$ with P,T and Q were recorded between 180 and 260 nm on a Chirascan CD spectrometer (applied Photophysics, UK). 100 µL of the peptide solution were added in a 0.1 mm path-length quartz cuvette, and the measurements were carried out at 20 °C (1 nm bandwidth resolution, and current time-per-point of 3 s). Typically, three scans were recorded, and baseline and PBS spectra were subtracted from each spectrum. Data were processed using Applied Photophysics chirascan Viewer at room temperature and neutral pH, which is in accordance with literature that confirms the typical β-sheet spectra [Yokoi et al., 2005].

2.7. Fourier-transform infrared spectroscopy (FT-IR)

FT-IR spectra were recorder on a Nicolet iS10 (ThermoScientific) Smart iTR spectrophotometer. The spectra were taken in the region 4000 and 500 cm^{-1} over 128 scans at a resolution of 4 cm^{-1} and an interval of 1 cm^{-1}. Here we show only the region 1740 and 1560 cm^{-1}, since that region shows the β-sheet structure, which was used to validate the CD results. Spectra of the ac-$(RADA)_4$-$CONH_2$ in PBS with and without drugs were recorded, and each spectrum was background subtracted.

3. Results and Discussion

3.1. AFM

To gain insight into the hydrogel's morphology, AFM was used providing clear support for self-assembly of peptides. Since RADA 16 is a peptide hydrogel with a secondary structure that is largely comprised of β-sheet, resulting in fibrils with diameters on the nanoscale, it can be defined as amyloid hydrogel [Knowles et al., 2010]. Confirming what the literature asserts, RADA 16 combined with the drug selected may form nanofibre that can be affected by changes depending on the drugs structure encapsulated into the hydrogel [Mains et al., 2013]. The images of drug loaded hydrogel (Fig. 2a-c) show that the addition of the chosen drug molecules has no distinct chaotropic or kosmotropic effect on the self-assembly of the functionalized peptides. The images detected from the combination between RADA16 and drugs, reveal morphological differences of nanostructures formed. In particular, two remarkably different morphologies of nanofibres were obtained from the interaction between RADA with P and Q (Fig.2a-b) and RADA with T (Fig.2c). P and Q loaded hydrogels show

no amyloid fibril formation producing a high density of nanofibres randomly distributed on the mica surface. The nanostructures consist of cross-linked network structures including elongated, thickened and twisted fibres. A large number of crosslinking points suggest a self-assembled into a denser network. T loaded hydrogel produces amyloid fibres in accordance with literature [Mains et al., 2013]. The formation of these fibres can be a potential consequence of a major mixed content between α-helix and β-sheet [VandenAkker et al., 2011] compared to the P and Q loaded RADA 16.

To quantitatively analyse the data, a large amount of the images has been examined in order to find the surface coverage of nanofibres, clusters and branches and further calculate the dimensions of nanofibres, which are reported in Table 3. The diameter of nanofibres for P and Q is the same confirming the similar interaction showed in Fig.2a-b between RADA 16 and drug loaded. The values carried out for P and Q show fibrous structures having width between a range of 6-8 nm, which is in excellent agreement with the molecular dimension of the β-sheet peptide [Zhao et al., 2009]. In direct contrast, T has larger fibres justifying the different arrangement indicated in Fig.2c. These results, despite the different interactions with the drugs selected, define RADA 16 as a unique candidate to easily incorporate hydrophobic drugs into the gel matrix due the capacity to keep an unchanged morphology of nanostructure after drugs encapsulation.

3.2. CD and FT-IR

During the drugs residence in the peptide solution, during self-assembly and nanofibre formation or during the release process, denaturation of hydrogel and destructive interaction between drugs and RADA16 could occur. To better understand the state of the peptides under different conditions, we have investigated their secondary structure using FT-IR and CD. Typical β-sheet spectra were observed at each point in time, indicating the molecular structure and the integrity of the peptides before and after the drug incorporation [Yokoi et al., 2005; Zhang et al.1995]. Fig.3 shows the CD spectra of RADA16 and drug loaded systems. Measurements were carried out in the visible and ultra-violet region of the electro-magnetic spectrum monitor electronic transitions. For all experiments, the analyses show a negative maximum at 220-221 nm and a positive maximum at 196 nm in concordance with literature values [Nagai et al., 2012]. Moreover, the characteristic peaks to describe α-helix approximately at 222 nm [Correa and Ramos, 2009] and β-sheet at 216 nm [Correa and Ramos, 2009] were analysed (Table 4). All CD spectra are consistent with β-sheet rich structures even after addition of drugs. The results suggest that at the molecular scale the individual peptides did not break into monomers but formed stable β-sheets and were packed together. The small differences in the ellipticity intensities that are observed in the CD spectra, propose that the elliptically polarized light when passed through the circular dichroic sample shows a different magnitude due to the characteristic absorbance of the samples selected [Uversky and Permyakov, 2007]. Furthermore, CD analysis reveals structural information which corroborates with the AFM images (Fig.2). The spectra for the P and Q perfectly follow the extended β-structure of the RADA 16. T, despite maintains a consistent secondary structure, shows a slightly different behaviour than the spectrum for RADA 16 without drug loaded. T spectrum shows a mixed content between α-helix and β-sheet [VandenAkker et al., 2011] compared to the other drug loaded systems (Table 4) permitting a completely different folding of hydrogel which is supported by the AFM image of observed fibres for the T system.

To validate the CD data further FT-IR spectroscopy has been used, since the formation of β-sheet-like structures can be monitored through the absorption of the amide group in FT-IR

spectroscopy. The FT-IR spectra (Fig.4), dashed line shows the signal for RADA16 without drug signal, and the continuous lines display the signal detected from interaction between drugs and peptide. In all experiments, before and after added drugs, a peak around 1616 cm^{-1} was detected. For conventional self-assembling peptides, a peak around 1615 cm^{-1} indicates the presence of aggregated β-sheets [Yokoi, 2005], [Zhang et al., 1995]. In the β-pleated sheet, the sheet-like structure is created by a series of hydrogen bonds between residues in different polypeptide chains or between residues in different sections of a folded polypeptide [Kumar et al., 2011]. Amide I bands at 1619 and 1616 cm^{-1} is the most structurally sensitive IR band; it mainly associated with the C=O stretching vibration and is directly related to the backbone conformation [Krimm and Bandekar, 1986]. The band at 1618 cm^{-1} is consistent with an antiparallel conformation, which shows that the fibres run in opposite directions [Kumar et al., 2011]. The band Amide II absorption peaks at 1526 and 1543 cm^{-1} results from the N-H bending vibration and from the C-N stretching vibration [Jackson and Mantsch, 1991]. In all spectra detected (Fig.4), the position of the peaks between spectra of RADA and RADA with drugs remains constant confirming the results obtained with CD. However, taking into consideration AFM results obtained, P and Q non-loaded amyloid fibres show similar amide I profiles to T loaded amyloid fibres but with slight differences in peak intensities. One evident discrepancy is visible in Fig.4 where the peak intensity of RADA with T, associated with β-sheet contribution, overhangs the peak of RADA 16 without drug loaded. Furthermore, in accordance with CD results, T amyloid fibre spectrum shows a different proportion of α-helix at 1637 cm^{-1} [Petty and Decatur, 2005] respect P and Q spectra.

3.3. Drug release

In order to further explore the potential of self-assembling peptide hydrogels as drug delivery system for hydrophobic drug molecules by proving a solution for delivery problems, it is imperative that the physicochemical characteristics of RADA16, the structural and the chemical properties of the drugs are taken into consideration.

The release of the drugs from the peptide nanofibre hydrogel is illustrated in Fig.5, as a plot of mass released fraction ($Mt/M\infty$) as a function of time (t). The model was developed assuming diffusion of small molecules, infinite dilution of the diffusant, and that the diffusion of the molecules through the hydrogel depends solely on Brownian motion [Koutsopoulous et al., 2008]. Racking one-dimensional solute release from a thin polymer slab of thickness where the initially drug concentration is maintained constant, a perfect sink condition is referred [Ritger and Peppas, 1986] providing a controlled release. These conditions permit to ignore the transport within the sink condition when calculating the overall release rate of the drug from the hydrogel [Nagai et al., 2005]. In the pharmaceutical field, several equations have been developed to model diffusional release from polymer [Rosema and Cardarelli, 1980] [Peppas, 1984], but the most acceptable expression to simplify the analysis of controlled release from various classical geometric shapes for non-swellable polymeric delivery systems was proposed by Peppas [Peppas, 1985] . Eq.4 is commonly used to determine apparent diffusion coefficients even when these conditions do not apply. The reason for doing this is that it facilitates the discussion of systems where there is no other easily transferable method for determining the diffusivity [Rosenbaum, 2011].

Furthermore, plotting the release data as function of the square root of time, Fig.6 shows a biphasic diffusion mechanism. The initial linear part of each plot indicates diffusion controlled release of the drugs from RADA16 and the diffusion coefficients were calculated following Eq.3 according with Fick's law. A deviation from the straight line at longer time is

evident after 4 hours ($t^{0.5}/s^{0.5}$: 120). This deviation from Fick behaviour may occur due the presence of hydrogel pores with small size and/or diffusion hindrance caused by specific interactions between diffusing drug molecules and peptide nanofibre of the hydrogel. In order to describe the non-linear regression model, SigmaPlot software was used to calculate the model parameters and the determination coefficients (R^2). There are several mathematical models to describe the kinetic profile of the considered drugs from the hydrogel formulation and to provide a good understanding of the drug dissolution [Costa and Lobo, 2000] [Kitazawa et al., 1977]. In this study three models were examined, using the equations presented in Table 2. The parameters calculated by these models and the determination coefficients (R^2) obtained are summarized in Table 5. The fit of each model was predicted based on some estimation: a) the dissolution profile described is a drug diffusion model for the case of diffusion of an initially uniformly distributed drug thought a polymeric matrix [Korsmeyer et al., 1983][Siepmann and Peppas, 2001]; b) the dissolution exponent (n) determines the dominant release mechanism and thus if $n \leq 0.43$ a Fickian diffusion is detected, if $0.43 \leq n \geq 0.85$ a non-Fickian diffusion is identified and if $n \geq 0.85$ a zero order is shown; c) when drug release is proportional to that remaining in the dosage form, dissolution can be described by first order release kinetics [Gibaldi and Feldman, 1967] [Wagner, 1969]; d) the Higuchi equation describes also the cumulative amount of released drug per unit area is proportional to the square root of time [Higuchi, 1963]. As it can be seen in Table 5, R^2 have similar value in more than one kinetic model and the dissolution rate constants reveal that Korsemeyer-Peppas is the predominant mechanism and fits the dissolution profiles. Following the literature [Boyapally et al., 2010], the goodness of fit for all models was based on comparisons of the higher R^2, smaller standard error of model parameters and smaller residual mean square for each model [Yuksel, 2000].

Fig.5 also shows the controlled release for all drug analysed in PBS and in BSS-Plus. Based on the release kinetics of the diffusing compounds we are able to categorize the drugs into: faster release drugs (T and P) and slower released drug (Q). Some of the release is sustained and a few faster because the formulation was not optimised showing a burst release and also it must be considered that the drug was not fully encapsulated in the hydrogels remaining on the surface.

A summary of the data analysis for the drugs released from RADA16 is presented in Table 6. The results show that the Stokes-Einstein equation ($D_{S\text{-}E}$: 3.33×10^{-10} for P; 2.82×10^{-10} for T; 4.71×10^{-11} for Q) overestimates the diffusivity of the drugs in solution. The reason for this discrepancy between the Stokes-Einstein diffusion coefficient and those determined by Eq.5 (D: $0.12 \pm 0.03 \times 10^{-10}$ for P; $0.16 \pm 0.04 \times 10^{-10}$ for T; $0.03 \pm 0.005 \times 10^{-11}$ for Q) is probably because in these experiments we used microliter drugs concentration. Hence, molecular crowding may have affected protein diffusion by slowing the molecular motion [Rosenbaum, 2011]. T and P present similar diffusivity values, while Q shows a considerably smaller value indicating an interaction between Q and the peptide fibres.

Fig.5a. shows the controlled release in PBS. The release profile shows the concentration of T in the supernatant increases quickly, more than 50 % of the loaded amount is released from the peptide scaffold in the first 1 h; T is released completely after 24 hours. Q was the slowest drug to be released in accordance with theoretical values and the initial hypothesis. P release reflects the T diffusion despite the longer time that it takes to leave the vehicle. P and T belong to the same pharmaceutical class of drugs, which means the pharmacophore is the same but with some structural differences, which can justified the delay in terms of delivery.

T in its structure presents a [1,2,5] thiadiazole group (Fig.1d) and P presents an indolic group (Fig.1b). Both rings are aromatics but according to the value of Bird structural index of aromaticity they have different values. The [1,2,5] thiadiazole has I=104 [Katritzky et al., 2010] and the P has a value of I=146 [Estrada, 2006]. These values describe a higher aromaticity character for P. Based on the high specific bindings between aromatic groups and matrix of RADA16; it is hypothesized that an aromatic ring could be responsible of prolonged release [Choi et al., 2008]. The same explanation can be used to rationalize the Q release. The drug contains a quinoline ring (Fig.1d) which has I=134 [Estrada, 2006] proving that quinoline ring is more aromatic than [1,2,5] thiadiazole group; so Q is slower than T. However, the difference of Bird index between P (I = 146) and Q (I = 134) suggests that P should be the slowest on lipophilic drug group; but Q has a major steric hindrance with 7 members ring (Fig.1d) which can reduce the diffusion capacity [Perale et al., 2012]. Furthermore it is likely to rationalize the order of release considering the pKa values of the drug selected (Table 1) and converting them into isoelectric points (pI). The pI values are 9.2 for P and T and 8.7 for Q. The pI of Q is closer to the pH value of the environment (7.4); this condition ensures a strongly interaction between Q and RADA16 peptide nanofibres [Nagai et al., 2006].

Data show that all drugs demonstrated a controlled release and their accumulated drug released were 100 % (P, T) and 20 % (Q). Despite Q is not totally out from the delivery system, the experiment was stopped after 7 days since was not significant differences between concentration released after 3 days and after 7 days. In BSS-PLUS (Fig.5b), the sequence of release is the same shown in PBS. BSS-PLUS keeps the same pH value of PBS but the composition is not only saline; here we also have dextrose. The presence of sugar theoretically could change the conditions of interaction between drugs and RADA16; however the present data show that it did not happen for the specific hydrogel. BSS-PLUS is a sterile intraocular irrigating solution and it copies the physiological conditions of eyes. This characteristic can be interesting for the study of T, which is frequently used in glaucoma therapy. In BSS-Plus T release from RADA16 is constant and sustained although after 7 days not all the drug is carried out from the hydrogel.

4. Conclusions

In this work, we investigate the possibility of using a hydrogel consisting of self-assembling peptides as a carrier for controlled drug release of lipophilic drugs. We screened P, T and Q functionalized with RADA16 (Ac-$(RADA)_4$-$CONH_2$) in two different solvents (PBS and BSS-PLUS). By using AFM we have demonstrated that the addition of functional drugs motif sequences has no distinct impediment on the self-assembly of the functionalized peptides despite the physicochemical characteristics of the drugs chosen can modify the morphology of the nanostructures. CD and FTIR demonstrated that RADA 16 adopts stable β-sheet structures and self-assembles also after addition of lipophilic drugs. We have shown that the release rate can be mainly controlled. Our data show that the release kinetics of the drugs analysed depends on their structure, on their chemical properties (e.g. LogP, pKa, pI, presence of aromatic rings, steric hindrance) and on the solvent chosen to study the release (e.g. PBS, BSS Plus). A sustained, controlled and efficient drug release has been achieved for lipophilic drugs from RADA16. Furthermore, the molecules with the same parameters (P and T) present similar behaviour in terms of drug release. These results indicate RADA16 as a "smart vehicle" to provide solutions for release problems associated with lipophilic drugs. The present study holds importance in the context of new drug delivery formulations, in order to optimize drugs performances.

References

Aggeli, A., Bell, M., Carrick, L. M., Fishwick, C.W., Harding, R., Mawer, P.J., Radford, S.E., Strong, A. E., Boden, N., 2003. pH as a trigger of peptide beta-sheet self-assembly and reversible switching between nematic and isotropic phases. J. Am. Chem. Soc. 125, 9619.

Altunbas, A., Lee, S.J., Rajasekaran, S.A., Schneider, J.P., Pochan, D.J., 2011. Encapsulation of curcumin in self-assembling peptide hydrogels as injectable drug delivery vehicles. Bioamterials. 32, 5906-5914.

Arosio, P., Owczarz, M., Wu, H., Butte´,A., Morbidelli, M., 2012. End-to-End Self-Assembly of RADA 16-I Nanofibrils in Aqueous Solutions. Biophysical Journal. 102, 1617–1626.

Boyapally, H., Nukala, R.K., Bhujbal, P., Douroumis, D., 2010. Controlled release from directly compressible theophylline buccal tablets. Colloids and Surfaces B: Biointerfaces. 77, 227–233.

Carrick, L.M., Aggeli, A., Boden, N., Fisher, J., Ingham, E., Waigh, T.A., 2007. Effect of ionic strength on the self-assembly, morphology and gelation of pH responsive beta-sheet tape-forming peptides. Tetrahedron. 31, 7457 – 7467.

Choi,W. I., Ihm, J., Kim, G., 2008. Modification of the electronic structure in a carbon nanotube with the charge dopant encapsulation. Appl. Phys. Lett. 92, 193110.

Corrêa, D. H. A., Ramos, C. H. I.,2009. The use of circular dichroism spectroscopy to study protein folding, form and function. Afr. J. Biochem. Res. 5, 164-173.

Costa, P., Lobo, J.M.S., 2000. Modelling and comparison of dissolution profiles. Eur J Pharm Sci. 13,123–133.

Eanes, E.D., Glenner, G.G., 1968. X-ray diffraction studies on amyloid filaments. J. Histochem Cytochem. 16, 673.

Estrada, Ernesto, 2006. On the Dimensionality of Aromaticity Criteria. Commun. Math. Comput. Chem. 56, 331-344.

Frisch, H.L., 1970. Diffusion in polymers edited by J. Crank and G. S. Park, Academic Press, London and New York, 1968. Journal of Applied Polymer Science. 12, 1657.

Gelain, F., Unsworth, L.D., Zhang, S., 2010. Slow and sustained release of active cytokines from self-assembling peptide scaffolds. J Control Release. 145, 231-239.

Gibas, I., Janik, H., 2010. Review: Synthetic polymer hydrogels for biomedical applications. Chemistry & Chemical technology. 4, 297-304.

Gibaldi, M., Feldman, S., 1967. Establishment of sink conditions in dissolution ratedeterminations. J. Pharm. Sci. 56, 1238–1242.

Hansch, C.; Leo, A.; Hoekman, D.H., 1995. Exploring QSAR, Fundamentals and Application in Chemistry and Biology. American Chemical Society: Washington, DC, USA.

Higuchi, T., 1963. Mechanism of sustained-action medication. Theoretical analysis of rate of release of solid drugs dispersed in solid matrices. J Pharm Sci. 52, 1145–1149.

Huang, R., Qi, W., Feng, L., Su, R., He, Z., 2011. Self-assembling peptide–polysaccharide hybrid hydrogel as a potential carrier for drug delivery. Soft Matter. 7, 6222–6230.

Jackson, M., Mantsch, H.H., 1991. Protein secondary structure from FT-IR spectroscopy: Correlation with dihedral angles from three-dimensional Ramachandran plots. Can. J. Chem. 69, 1639–1642.

Jayawarna, V., Ali, M., Jowitt, T.A., Miller, A.E., Saiani, A., Gough, J.E., Ulijn, R.V., 2009. Self-assembly and hydrogelation promoted by F5-phenylalanine. Adv. Mater. 18, 611-614.

Jonker, A. M., Loewik, D. W. P. M., van Hest, J. C. M., 2012. Peptide and Protein-Based Hydrogels. Chem. Mater. 24, 759– 773.

Jun, S., Hong, Y., Chen, P., 2004. Self-assembly of the ionic peptide EAK16: the effect of charge distributions on self-assembly. Biophys. J. 87, 1249–1259.

Katritzky, A. R., Ramsden, C. A., Joule, J. A., Zhdanki, V.V., 2010. Handbook of Heterocyclic Chemistry, third ed, Elsevier Ltd, Amsterdam.

Keyes, C., Duhamel, J., Fung, S.Y., Bezaire, J., Chen, P., 2004. Release of a Hydrophobic Cargo Microencapsulted with EAK16 II into Membrane Bilayers. J. Am. Chem. Soc. 126, 7522-7532.

Kitazawa, S., Johno, I., Mihouchi, T., Okada, J.,1977. Interpretation of dissolution rate data from in vitro testing of compressed tablets. J Pharm Pharmacol. 29, 453–459.

Knotturi, A.K., Murtomaki, L., Schiffrin, D.J., 1992. An electrochemical study of long chain aliphatic amines. Acta Chemica Scandinavica, 46, 47-53.

Knowles, T. P. J., Oppenheim, T.W., Buell, A. K., Chirgadze, D.Y., Welland, M. E., 2010. Nat. Nanotechnol. 5, 204–207.

Korsmeyer, R.W., Gurny, R., Doelker, E.M., Buri, P., Peppas, N.A., 1983. Mechanism of solute release from porous hydrophilic polymers. Int. J. Pharm. 15, 25–35.

Koutsopoulos, S., Unswortha, L. D., Nagaia, Y., Zhanga, S., 2008. Controlled release of functional proteins through designer self-assembling peptide nanofiber hydrogel scaffold. PNAS. 106, 4623–4628.

Krimm, S., Bandekar, J., 1986. Vibrational spectroscopy and conformation of peptides, polypeptides, and proteins. Adv Protein Chem. 38, 181–364.

Kumar, P., Pillay, V., Modi, G., Choonara, Y. E., du Toit, L. C., Naidoo, D. 2011. Self-Assembling Peptides: Implications for Patenting in Drug Delivery and Tissue Engineering. Recent Patents on Drug Delivery & Formulation. 1, 24-51.

Mains, J., Lamprou, D. A., McIntosh, L., Oswald, I. D. H, Urquhart, A. J., 2013. Beta-adrenoceptor antagonists affect amyloid nanostructure; amyloid hydrogels as drug delivery vehicles. Chem. Commun. 49, 5082-5084.

Misra, H., Mehta, B.K., Jain, D.C., 2008. Optimization of Extraction Conditions and HPLC - UV Method for Determination of Quinine in Different Extracts of Cinchona species Bark. Rec. Nat. Prod. 2, 107-115.

Nagai, Y., Unsworth, L.D., Koutsopoulos, S., Zhang, S., 2006. Slow release of molecules in self-assembling peptide nanofiber scaffold. J.Controlled release. 115, 18–25.

Nagai,Y., Yokoi, H., Kaihara, K., Naruse, K., 2012. The mechanical stimulation of cells in 3D culture within a self-assembling peptide hydrogel. Biomaterials. 33, 1044-1051.

Nune, M., Kumaraswamy, P., Maheswari Krishnan, U., Sethuraman, S., 2013. Self-Assembling Peptide Nanofibrous Scaffolds for Tissue Engineering: Novel Approaches and Strategies for Effective Functional Regeneration. Current Protein and Peptide Science. 14, 70-84.

Peppas, N.A., 1984. Mathematical modelling of diffusion processes in drug delivery polymeric systems. Controlled Drug Bioavailability, Vol. 1. Drug Product Design and Performance, Wiley. New York, p. 203.

Peppas, N.A., 1985. Analysis of Fickian and non-Fickian drug release from polymers. Pharm. Acta Helv. 60, 110.

Perale, G., Rossi, F., Santoro, M., Peviani, M., Papa, S., Liupi, D., Torriani, P., Micotti, E., Previdi, S., Cervo, L., Sundrom, E., Boccaccini, A.R., Masi, M., Forloni, G., Veglianese, P., 2012. Multiple drug delivery hydrogel system for spinal cord injury repair strategies. J. Controlled release. 159, 271-80.

Petty, S. A., Decatur, S. M., 2005. Experimental evidence for the reorganization of beta-strands within aggregates of the Abeta (16-22) peptide. J. Am. Chem. Soc. 127, 13488–13489.

Ramachandran, S., Taraban, M.B., Yu, Y.B., 2005. Repeated rapid shear-responsiveness of peptide hydrogels with tunable shear modulus. Biomacromolecules. 6, 1361-1321.

519 Ritger, P.L., Peppas, N.A., 1987. A Simple Equation for Description of Solute Release. II.
520 Fickian and Anomalous Release from Swellable Devices. J. Controlled Release. 5, 37-42.
521 Rosenbaum, Sara, 2011. Basic Pharmacokinetics and Pharmacodynamics: An Integrated
522 Textbook and Computer Simulation, John Wiley & Sons, New Jersey.
523 Roseman, T.J, Cardarelli, N.F., 1980. Monolithic polymer devices. Controlled Release
524 Technologies. Vol. 1, CRC Press, Boca Raton.
525 Sharma, N., Singh Rao, S., Reddy A. M., 2012. A Novel and Rapid Validated Stability-
526 Indicating UPLC Method of Related Substances for Dorzolamide Hydrochloride and Timolol
527 Maleate in Ophthalmic Dosage Form. J. of Chromatographic Science. 50, 745–755.
528 Siepmann, J., Ainaoui, A., Vergnaud, J.M., Bodmeier, R., 1998. Calculation of the
529 dimensions of drug-polymer devices based on diffusion parameters. J. Pharm. Sci. 87, 827–
530 832.
531 Siepmann, J., Peppas, N.A., 2001. Modeling of drug release from delivery systems based on
532 hydroxypropyl methylcellulose (HPMC). Advanced Drug Delivery Reviews. 48, 139–157.
533 Srinivas, M., Hopperstad M.G., Spray, D.C., 2001. Quinine blocks specific gap junction
534 channel subtypes. PNAS. 98, 10942–10947.
535 Uversky, V. N., Permyakov, E. A., 2007. Methods in Protein Structure and Stability
536 Analysis: Luminescence Spectroscopy and Circular Dichroism, Nova Science Publisher, New
537 York.
538 Vahdat, N., Sullivan, V.D., 2001. Estimation of permeation rate of chemicals through
539 elastometric materials, J. Appl. Polym. Sci. 79, 1265–1272.
540 VandenAkker, C. C., Engel, M. F. M., Velikov, K. P., Bonn M., Koenderink, G. H., 2011.
541 Morphology and Persistence Length of Amyloid Fibrils Are Correlated to Peptide Molecular
542 Structure. J. Am. Chem. Soc. 133, 18030–18033.
543 Wagner, J.G., 1969. Interpretation of percent dissolved-time plots derived form in vitro
544 testing of conventional tablets and capsules. J. Pharm. Sci. 18, 1253–1257
545 Wildt, D., Sangster, B., Langemeijer, J., de Groot, G., 1984. Different toxicological profiles
546 for various beta- blocking agents on cardiac function in isolated rat hearts. J. Toxicol. Clin.
547 Toxicol. 22, 115-132.
548 Xu, A., Madden, T., 2011. Analytical methods for therapeutic drug monitoring and
549 toxicology. First ed., John Wiley & Sons, New Jersey.
550 Yokoi, H., Kinoshita, T., Zhang, S., 2005. Dynamic reassembly of peptide RADA16
551 nanofiber scaffold. Proc. Natl. Acad. Sci. USA. 102, 8414–8419.
552 Yuksel, N., Kanik, A.E., Baykara, T., 2000. Comparison of in vitro dissolution profiles by
553 ANOVA-based, model-dependent and independent methods. Int J Pharm. 209, 56–67.
554 Zhang Shuguang, 2002. Emerging biological materials through molecular self- assembly.
555 Biotech Adv. 20, 321-39.
556 Zhang, Shuguang, 2003. Fabrication of novel materials through molecular self-assembly.
557 Nature Biotechnology. 21, 1171-1178.
558 Zhang, S., Holmes, S., Lockshin, C., Rich, A., 1993. Spontaneous assembly of a self-
559 complementary oligopeptide to form a stable macroscopic membrane. Proceedings of
560 National Academy of Science USA. 90, 3334-3338.
561 Zhang, S., Holmes, T., DiPersio, M., R.O. Hynes, Su, X., Rich, A., 1995. Self-
562 complementary oligopeptide matrices support mammalian cell attachment. Biomaterials. 16,
563 1385–1393.
564 Zhang, S., Marini, D.M., Santoso, S., 2002. Design of nanostructured biological materials
565 through self-assembly of peptides and proteins. Curr. Opin. Chem. Biol. 6, 865–871.
566 Zhao, Y., Tanaka, M., Kinoshita, T., Higuchi, M., Tan, T., 2009. Nanofibrous scaffold from
567 self-assembly of β-sheet peptides containing phenylalanine for controlled release. Journal of
568 Controlled Release 142, 354–360.

569 Zhaoyang, Y., Zhang, H., Luo, H., Wang, S., Zhou, Q., Du, X., Tang, C., Chen, L., Liu, J.,
570 Shi, Y., Zhang, E., Behnk, R., Zhao, X., 2008. Temperature and pH effects on biophysical
571 and morphological properties of self-assembling peptide RADA16-I. J. Pept. Sci. 10, 1002.

Figures legend:

Fig.1. Chemical structures of the compounds used. a) Pindolol (P), b) Quinine (Q), and c) Timolol maleate (T).

Fig.2. AFM images obtained from peptide RADA16 networks at scale 3.5 µm x 3.5 µm. a) RADA16 with P, b) RADA16 with Q, c) RADA16 with T, d) only RADA16 with an additional image at 250nm of scale bar.

Fig.3. CD spectra of RADA16 with and without incorporated P, Q and T. RADA16 peptide had a typical β-sheet structure. When drugs were incorporated with RADA16, there was not any change in β-sheet structure.

Fig.4. FT-IR spectra of RADA 16 with and without incorporated P, Q and T. The dashed line shows the signal for RADA16 without drug signal; the continuous lines display the signal for interaction between RADA16 and drugs.

Fig.5. Cumulative release of P, Q and T. a) in PBS and b) in BSS-Plus.

Fig.6. Linear fit obtained from drugs release of P, Q and T. a) PBS and b) BSS-Plus.

591 **Fig.1.**

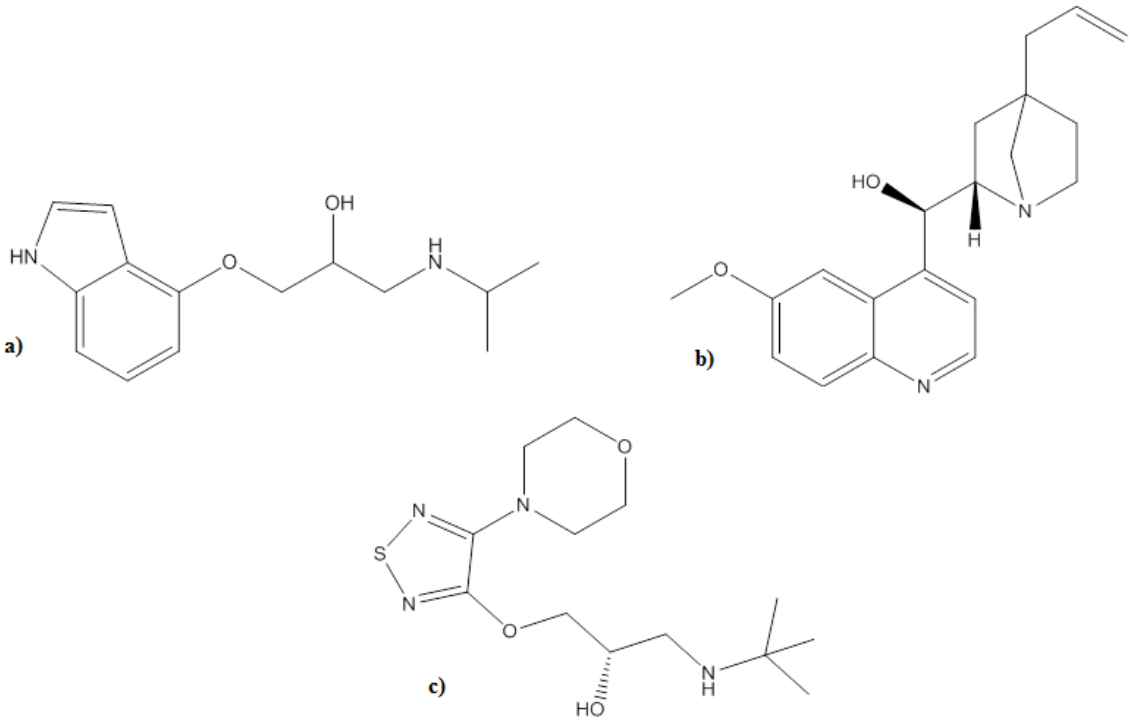

592

593 **Fig.2.**

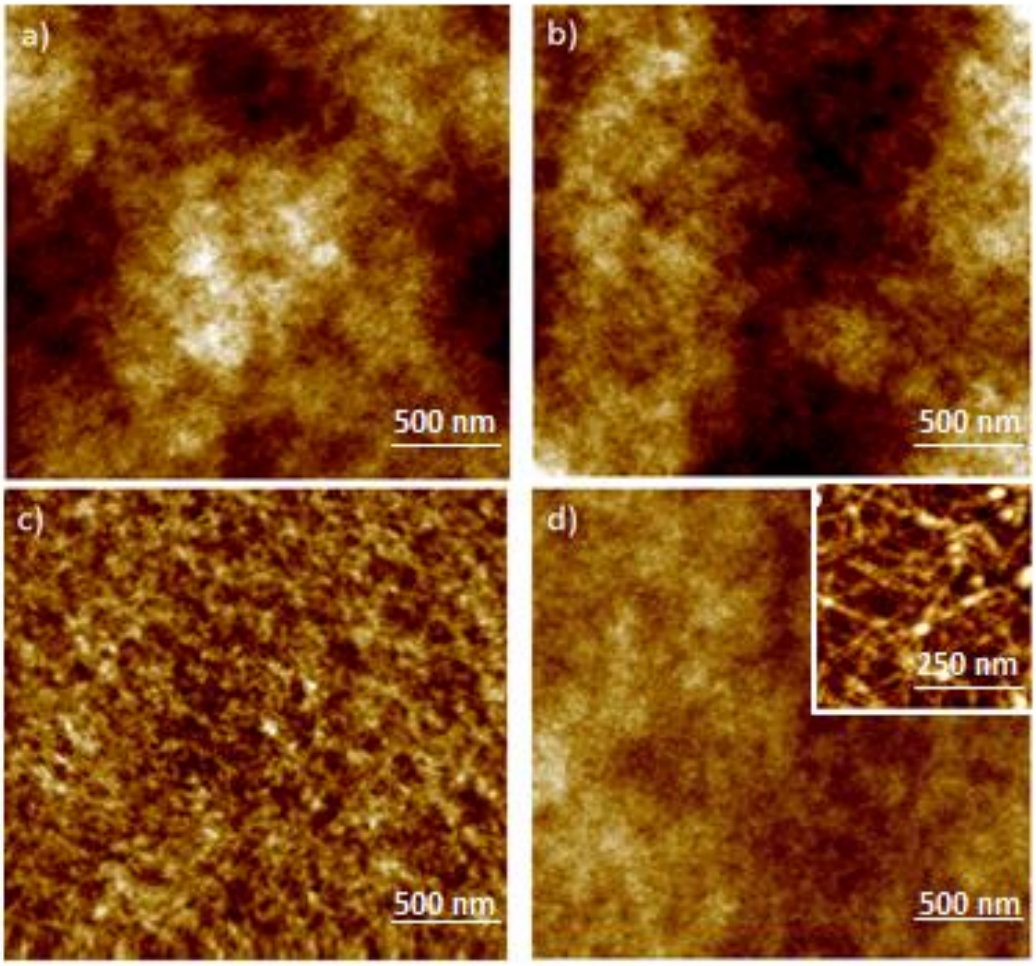

594
595

596 **Fig.3.**
597

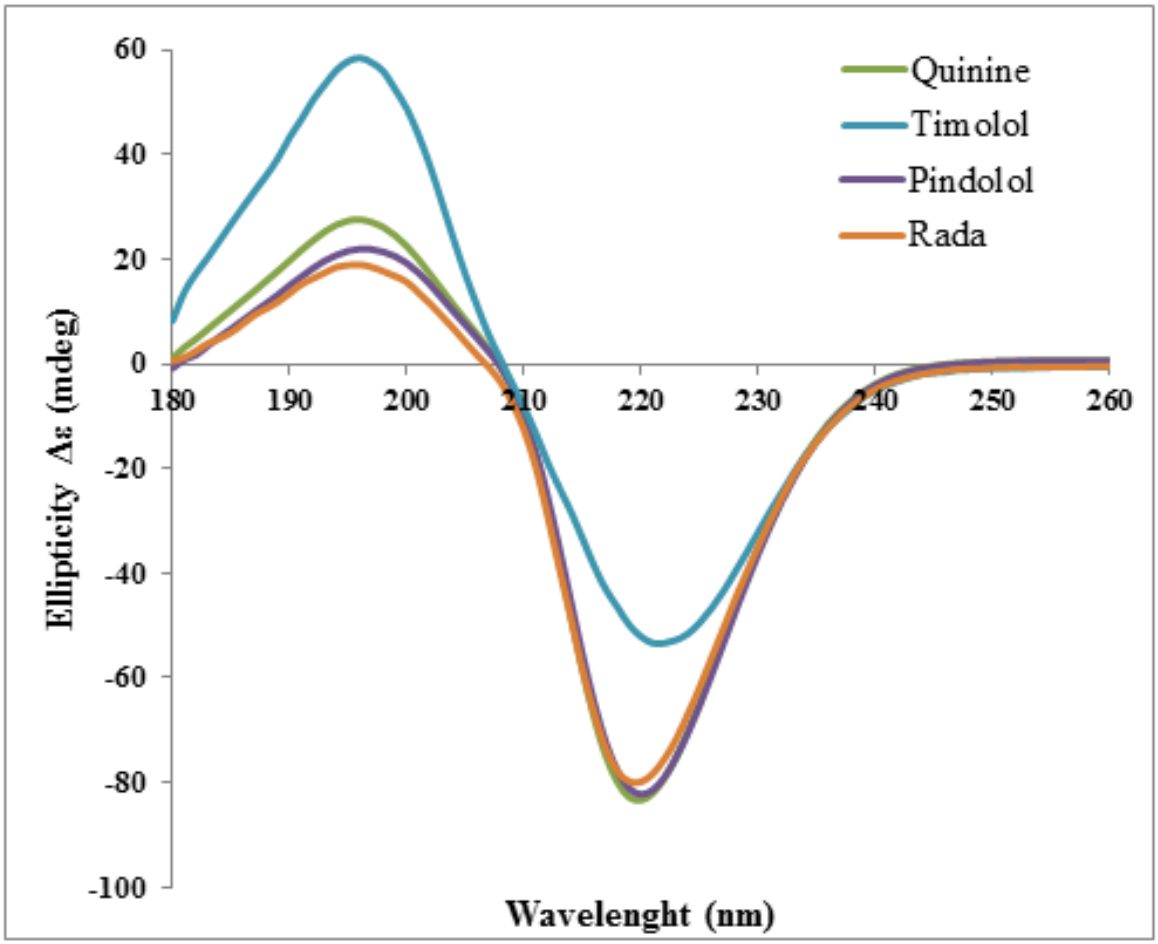

598

599 **Fig.4.**
600

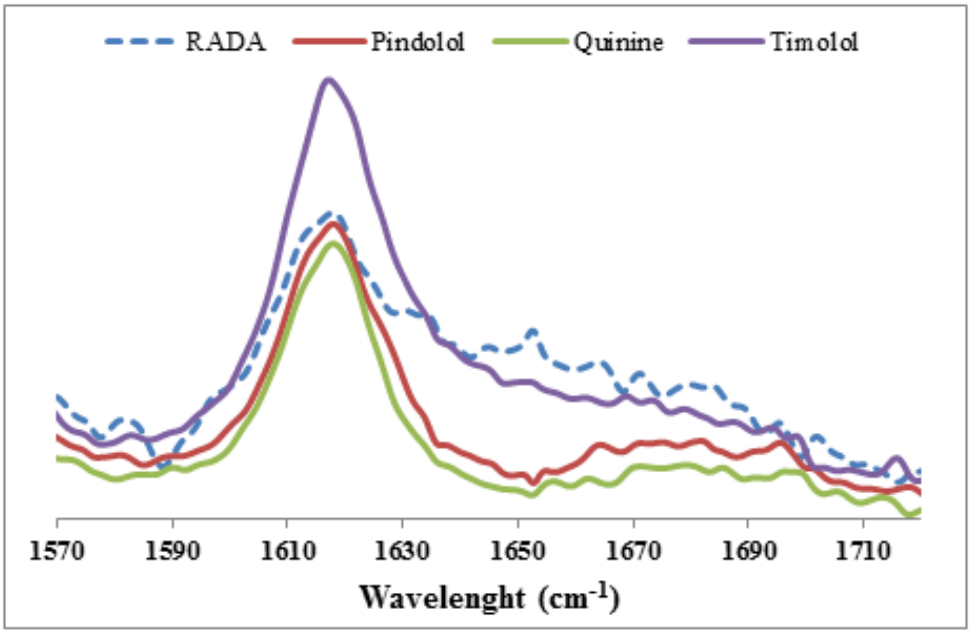

601
602
603

Fig.5

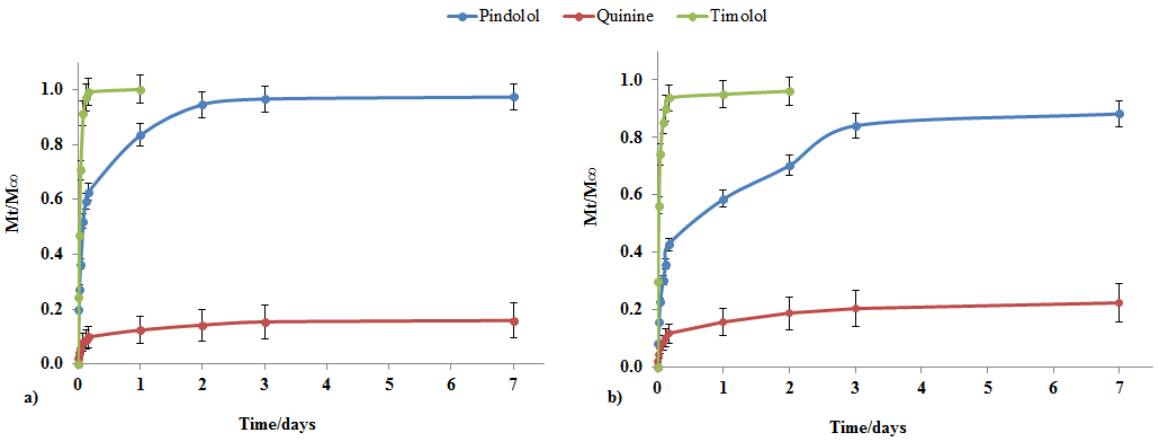

608 **Fig.6**

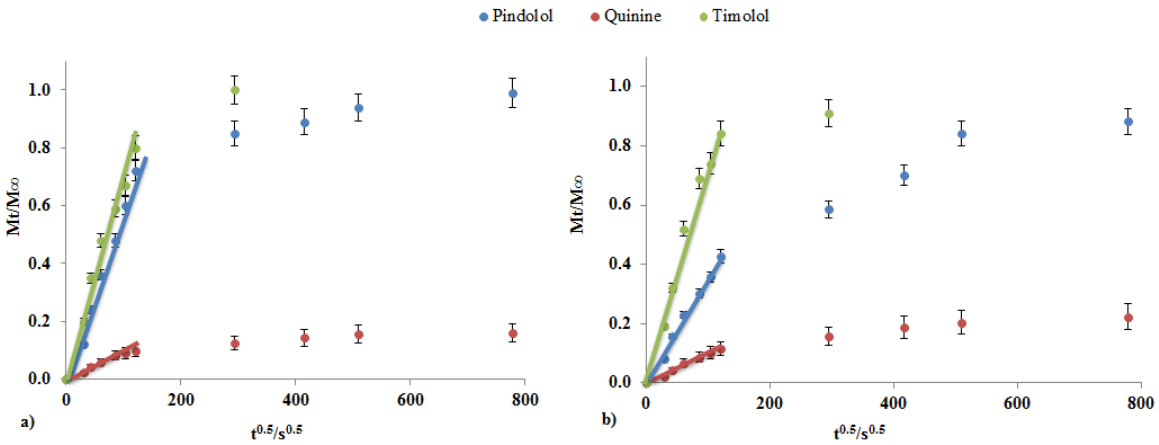

609
610

Tables:

Table 1. List of drugs used in this work with their physicochemical properties.

	Compound	Symbol	Purity	MW	LogP	pKa	λ max (nm)
a)	Pindolol	P	≥ 98%	248.32	1.97 [Rosenbaum, 2011]	9.25 [Wildt et al., 1984]	220 [Xu et al., 2011]
b)	Quinine	Q	90%	327.44	3.44 [Hansh et al., 1995]	8.7 [Srinivas et al., 2001]	225 [Misra et al., 2008]
c)	Timolol Maleate	T	≥ 98%	316.42	1.83 [Sharma et al., 2012]	9.21 [Knotturi et al., 1992]	295 [Ramachandran et al., 2005]

618 **Table 2.** Applied dissolution models.

Model	Equation
First order	$M_t = M_0\, e^{-kt}$
Higuchi	$M_{L,t} = k_H\sqrt{t}$
Korsmeyer-Peppas	$F = k_p t^n$

619 F, amount of drug dissolved in time t; k and k_p dissolution rate constants; n dissolution
620 exponent.

621 **Table 3.** Values of dimension of nanofibres (d) and values of surface roughness (Ra)
622 obtained from AFM analysis.
623

Sample	d / nm	R_a / nm
RADA	12.24 ± 1.09	0.53 ± 0.23
P	7.76 ± 0.7	0.38 ± 0.10
Q	7.57 ± 0.68	0.41 ± 0.16
T	10.62 ± 0.74	0.46 ± 0.22

624

625 **Table 4.** Values obtained from CD analysis for each experiment.
626

	P ($cm^2 \cdot dmol^{-1}$)	**Q** ($cm^2 \cdot dmol^{-1}$)	**T** ($cm^2 \cdot dmol^{-1}$)	**RADA 16** ($cm^2 \cdot dmol^{-1}$)
Positive maximum	$[\theta]_{196} = 21.98$	$[\theta]_{196} = 27.61$	$[\theta]_{196} = 58.49$	$[\theta]_{196} = 18.98$
Negative maximum	$[\theta]_{220} = -82.16$	$[\theta]_{221} = -82.00$	$[\theta]_{220} = -53.35$	$[\theta]_{220} = -79.85$
α-helix	$[\theta]_{222} = -78.94$	$[\theta]_{222} = -79.12$	$[\theta]_{222} = -53.35$	$[\theta]_{222} = -75.43$
β- sheet	$[\theta]_{216} = -72.43$	$[\theta]_{216} = -75.04$	$[\theta]_{216} = -43.16$	$[\theta]_{216} = -73.61$

627

628 **Table 5.** Dissolution rate constants and determination coefficients of drug released from
629 hydrogel formulations.
630

Model		Pindolol	Quinine	Timolol
First order	k	$2.1x10^{-2}$±$6.3x10^{-3}$	$5.4x10^{-3}$± $4.0x10^{-4}$	$3.7x10^{-3}$± $2.4x10^{-4}$
	R^2	0.9748	0.9821	0.9783
Higuchi	k_H	7.048 ± 0.441	4.387 ± 0.354	2.837 ± 0.197
	R^2	0.9865	0.9880	0.9745
Peppas	k_p	6.698 ± 0.074	2.985 ± 0.033	4.394 ± 0.087
	R^2	0.9983	0.9904	0.9951

631

632 **Table 6.** Diffusion parameters and calculated values for the compounds released from
633 RADA16.
634

	P	**T**	**Q**
Volume / l	0.2 ± 0.01	0.2 ± 0.01	0.2 ± 0.01
H / m	$4.2 \pm 0.04 \times 10^{-3}$	$4.2 \pm 0.04 \times 10^{-3}$	$4.2 \pm 0.04 \times 10^{-3}$
r_h / m	6.8×10^{-9}	80×10^{-9}	48×10^{-9}
D / m^2 s^{-1}	$0.12 \pm 0.03 \times 10^{-10}$	$0.16 \pm 0.04 \times 10^{-10}$	$0.03 \pm 0.005 \times 10^{-11}$
D_0 / m^2 s^{-1}	$0.05 \pm 0.02 \times 10^{-10}$	$0.07 \pm 0.02 \times 10^{-10}$	$0.004 \pm 0.0001 \times 10^{-11}$
D_{S-E} / m^2 s^{-1}	3.33×10^{-10}	2.82×10^{-10}	$4{,}71 \times 10^{-11}$
B	0.07	0.09	0.05
J / µg m^{-2} s^{-1}	1.7×10^{-8}	1.87×10^{-8}	2.38×10^{-10}

635
636